Four-wave mixing in Weyl semimetals

Sultan Almutairi,[1] Qianfan Chen,[1] Mikhail Tokman,[2] and Alexey Belyanin[1]
[1]*Department of Physics and Astronomy, Texas A&M University, College Station, Texas 77843, USA*
[2]*Institute of Applied Physics, Russian Academy of Sciences, Nizhny Novgorod, 603950, Russia*

(Received 27 April 2020; accepted 12 June 2020; published 23 June 2020)

Weyl semimetals (WSMs) have unusual optical responses originating from unique topological properties of their bulk and surface electron states. Their third-order optical nonlinearity is expected to be very strong, especially at long wavelengths, due to linear dispersion and high Fermi velocity of three-dimensional Weyl fermions. Here we derive the third-order nonlinear optical conductivity of WSMs in the long-wavelength limit and calculate the intensity of the nonlinear four-wave mixing signal as it is transmitted through the WSM film or propagates away from the surface of the material in the reflection geometry. All results are analytic and show the scaling of the signal intensity with variation of all relevant parameters. The nonlinear generation efficiency turns out to be surprisingly high for a lossy material, of the order of several mW per W^3 of the incident pump power. Optimal conditions for maximizing the nonlinear signal are realized in the vicinity of bulk plasma resonance. This indicates that ultrathin WSM films of the order of skin depth in thickness could find applications in compact optoelectronic devices.

DOI: 10.1103/PhysRevB.101.235156

I. INTRODUCTION

Weyl semimetals (WSMs) are fascinating materials with nontrivial topology of both bulk and surface electron states [1–8]. Although most of the research on WSMs has been focused on their electronic structure and transport, a number of recent studies have suggested that WSMs should also have highly unusual optical properties; see, e.g., Refs. [9–22] and references therein. Their optical response can be used to provide detailed spectroscopic information about their electronic structure, which is in a sense complementary to the one obtained from transport studies. Furthermore, strong anisotropy and gyrotropy of their optical response in combination with strong optical nonlinearities [18,22,23] makes WSM films promising for applications in optoelectronics and quantum technologies.

Due to the presence of one or more pairs of separated Weyl nodes, the electron band structure of WSMs is anisotropic and includes both bulk and surface states. As a result, even in the weak-field linear regime, the optical conductivity tensor is quite complicated and generally cannot be expressed analytically even within the simple microscopic model of a two-band WSM Hamiltonian with two separated Weyl nodes ([2,24]); see, e.g., Refs. [18,22] where bulk and surface conductivity tensors were derived and the properties of bulk and surface electromagnetic eigenmodes were described. Fortunately, one expects the strongest nonlinear optical response in the high-doping, long-wavelength limit $\hbar\omega \ll 2E_F, \hbar v_F b$, where E_F is the Fermi energy and $2\hbar b$ is the Weyl point separation in momentum space [18]. In this limit, the electron band structure takes a simple universal form of 3D cones for both Dirac and Type-I WSMs. As a result, one can obtain analytic, although a bit cumbersome, expressions for the nonlinear conductivity of any order.

There are several reasons why the power of the nonlinear four-wave mixing (FWM) efficiency from WSMs should be high in the long-wavelength limit. First, the dispersion of massless Weyl fermions is, of course, very far from parabolic, which ensures strong nonlinearity of intraband electron oscillations in an external optical field. This is to be contrasted with electrons near the conduction band minimum of conventional semiconductors that are only weakly nonparabolic: see, for example, Refs. [25–27] where the third-order intraband nonlinear response due to band nonparabolicity has been observed and explained.

Second, the magnitude of the dipole matrix element of the optical transitions between two states $|n\rangle$ and $|m\rangle$ with eigenenergies ε_n and ε_m is $\vec{\mu}_{mn} = e \cdot \langle m|\mathbf{r}|n\rangle = \frac{i\hbar e}{\varepsilon_n - \varepsilon_m}\langle m|\hat{\mathbf{v}}|n\rangle$. For electron systems with continuous energy spectra, the main contribution to the optical response at frequency ω comes from energy states separated by $\varepsilon_n - \varepsilon_m = \hbar\omega$. Furthermore, for massless fermions, the magnitude of the velocity is constant: $\hat{\mathbf{v}} = v_F\hat{\vec{\sigma}}$, i.e., $|\mathbf{v}| = v_F$, where v_F is the Fermi velocity. Therefore, the magnitude of the dipole moment scales as $\mu \sim ev_F/\omega$. This is true for both intraband and interband transitions. Note the linear scaling with wavelength λ, $\mu \propto \lambda$ for Weyl fermions as compared to the usual $\mu \propto \sqrt{\lambda}$ scaling for massive electrons with parabolic dispersion. As a result, the nonlinear nth order conductivity grows rapidly, $|\sigma^{(n)}| \propto \mu^{n+1}$, with increasing wavelength. Taking into account the density of states, one can immediately predict the scaling $|\sigma^{(3)}| \propto \frac{e^4 v_F}{(\hbar\omega)^3}$, which is confirmed below. The resulting magnitude of $|\chi^{(3)}|$ is many orders of magnitude higher than in conventional nonlinear materials.

The third reason is that at low frequencies $\hbar\omega \ll 2E_F$, the interband absorption is eliminated by Pauli blocking. Finally, the electric field of the nonlinear signal is enhanced in the vicinity of bulk plasma resonance due to the boundary

conditions at the interface. The latter effect is similar to the observed enhancement of Kerr index modulation and third-harmonic generation in so-called epsilon-near-zero materials; see, e.g., Refs. [28,29]. An exceptionally high value of $|\chi^{(3)}|$ in combination with field enhancement at plasma resonance lead to a surprisingly high efficiency of the nonlinear generation, of the order of several mW per W^3 of incident pump power.

The third-order conductivity has been calculated in Ref. [30] in the hydrodynamic limit and for frequencies lower than the scattering rate $1/\tau$. Here we are interested in the frequencies higher than the scattering rate, but still low enough to limit the response to the vicinity of the Weyl points, as argued above. Therefore, we need to use the kinetic approach. There is some controversy surrounding the kinetic theory of the third-order response. In Ref. [31], the third-order conductivity in the terahertz spectral range was calculated for degenerate FWM ($\omega + \omega - \omega$) and third-harmonic generation processes. However, in a very recent paper [32], the third-order conductivity was found to be zero in the low-frequency limit and the zero result was rationalized by symmetry arguments. While the inversion symmetry prohibits the nonzero *second-order* response in electric-dipole approximation, we don't see any symmetry arguments that would require the third-order response of WSMs to be zero, even assuming perfectly isotropic conical dispersion near every Weyl point. And indeed, we present a very general kinetic equation-based derivation of the third-order conductivity to show that it remains finite and in fact quite large in magnitude at low frequencies.

In Sec. II of this paper, we derive the general expression for the third-order nonlinear conductivity by using the kinetic equation formalism for frequencies higher than the phenomenological relaxation rate. We then proceed in Sec. III to calculate the FWM signal power transmitted through a WSM slab or propagating away from the surface of the material opposite to the direction of incident pump beams as a function of relevant parameters. The Appendix contains details of the derivation of the third-order susceptibility.

II. THIRD-ORDER NONLINEAR OPTICAL CONDUCTIVITY

We consider the optical response of a doped WSM at frequencies $1/\tau < \hbar\omega < 2E_F$ that are low enough so the electron excitations in the vicinity of each Weyl point satisfy the linear dispersion,

$$E_s = s\mathbf{v}\cdot\mathbf{p}, \tag{1}$$

where $s = \pm 1$ is for the conduction and valence bands, respectively. We assume for simplicity that the velocity has the same magnitude in every direction, i.e., the cone is isotropic. Anisotropic cones can be easily incorporated into the analytic theory below, but they will make the expressions more cumbersome without changing the nonlinear response qualitatively. We will assume for definiteness that the Fermi level is in the conduction band. Thus we have

$$\mathbf{v} = \frac{\partial E_+}{\partial \mathbf{p}} = v_F\mathbf{n}, \tag{2}$$

where E_+ is the electron energy in the conduction band, $p = \sqrt{p_x^2 + p_y^2 + p_z^2}$ is the magnitude of electron momentum, and $\mathbf{n} = \frac{\mathbf{p}}{p} = (\sin\theta\cos\phi, \sin\theta\sin\phi, \cos\theta)$ is the unit vector in the direction of the electron velocity in spherical coordinates. For $\hbar\omega < 2E_F$ and in the limit of strong Fermi degeneracy, intraband transitions make the dominant contribution. When only the intraband transitions are included, the fully quantum approach based on the von Neumann equation for the density matrix gives the same result as the semiclassical kinetic equation approach. For massless 2D Dirac fermions, this was checked explicitly in Ref. [33]. The kinetic equation with a phenomenological collision term has a standard form,

$$\frac{\partial f}{\partial t} + v_F(\mathbf{n}\cdot\nabla)f - e[\mathbf{E} + \frac{v_F}{c}(\mathbf{n}\times\mathbf{B})]\cdot\frac{\partial f}{\partial \mathbf{p}} = \gamma[F(p) - f], \tag{3}$$

where $\mathbf{E}$ and $\mathbf{B}$ are external electric and magnetic fields, respectively, γ is the electron relaxation rate, $F(p)$ is an unperturbed (zeroth order) distribution function, which is chosen as the equilibrium Fermi-Dirac distribution, and f is the nonequilibrium distribution function in the presence of external fields. We are interested in the electric-dipole optical response, so we will neglect the magnetic-field-dependent terms and the terms with spatial gradients in Eq. (3). The latter would lead to corrections that scale as powers of the small parameter $v_F/(L\omega)$, where L is a characteristic scale of the optical field nonuniformity in the material [33,34]. In a transparent medium, L would be equal to the wavelength of radiation.

The current density can be calculated as

$$\mathbf{j}(\mathbf{r}, t) = -e\int \mathbf{v} f(\mathbf{r}, \mathbf{p}, t)\, d^3p. \tag{4}$$

We assume that the electric field has the form

$$\mathbf{E}(\mathbf{r}, t) = \sum_n \mathbf{E}_n(\mathbf{r}, \omega_n)e^{-i\omega_n t} = \sum_n \mathbf{A}_n e^{ik_n z - i\omega_n t}, \tag{5}$$

and make an ansatz for the nonequilibrium distribution function,

$$f = \sum_m \xi_m e^{iq_m z - i\omega_m t}, \tag{6}$$

where we have set $\xi_0 = F(p)$, $E_0 = 0$, $\omega_0 = q_0 = 0$. Because both the electric field and the nonequilibrium distribution function are real, i.e., $\mathbf{E}(\mathbf{r}, t) = \mathbf{E}^*(\mathbf{r}, t)$ and $f = f^*$, we obtain $E_{-n} = E_n^*$, $\xi_{-n} = \xi_n^*$, $\omega_{-n} = -\omega_n$, $q_{-n} = -q_n$.

Substituting Eqs. (5) and (6) into Eq. (3) and transforming into spherical coordinates, one can solve for the distribution function in any required order and then perform an integration in Eq. (4) to find the nonlinear current. The details of the derivation are in the Appendix. The resulting third-order nonlinear optical conductivity tensor at frequency $\omega_n = \omega_1 + \omega_2 + \omega_3$ has the form

$$\sigma_{ijkl} = \frac{e^4 v_F g_s g_w \Delta_{ijkl}}{90\pi^2\hbar^3(\gamma - i\omega_1)} \times \frac{1}{[\gamma - i(\omega_1+\omega_2)][\gamma - i(\omega_1+\omega_2+\omega_3)]} + \text{all permutations of } \omega_1, \omega_2, \omega_3, \tag{7}$$

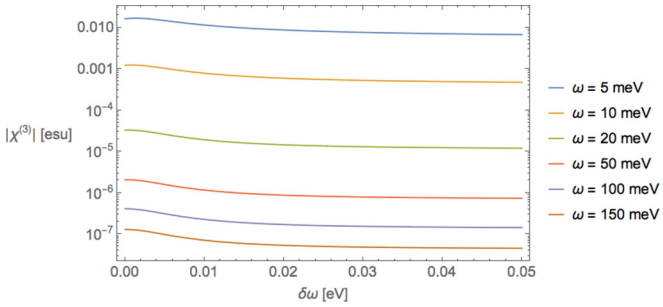

FIG. 1. The absolute value of $\chi^{(3)}$ as a function of detuning $\delta\omega = \omega_2 - \omega_1$ for several values of ω_1. Other parameters are $\hbar\gamma = 5$ meV, $v_F = 10^8$ cm/s, $g_s = 2$, $g_w = 4$.

where $\Delta_{ijkl} \equiv \delta_{ij}\delta_{kl} + \delta_{ik}\delta_{jl} + \delta_{il}\delta_{jk}$. Here, δ_{ij} is the Kronecker delta.

In the particular case of the third-harmonic generation, $\omega_1 = \omega_2 = \omega_3 = \omega$. Then the nonlinear current at $\omega_n = 3\omega$ is

$$j_k^{(3)}(3\omega) = \frac{e^4 v_F g_s g_w \left(E_{1,x}^2 + E_{1,y}^2 + E_{1,z}^2\right)}{5\pi^2\hbar^3(\gamma - i3\omega)(\gamma - i2\omega)(\gamma - i\omega)} E_{1,k}, \quad (8)$$

where $k = (x, y, z)$. This is consistent with the result for $\sigma_3^{\text{intra}}(3\omega)$ in Ref. [31] when $E_{1,x,y,z} = E_0$.

In another special case of partially degenerate FWM, we consider the nonlinear current at frequency $\omega_s = 2\omega_1 - \omega_2$. For simplicity, we assume that the electric field is along the z axis; then the z component of the nonlinear current is

$$j_z^{(3)}(\omega_s) = \frac{e^4 v_F g_s g_w E_{1,z}^2 E_{2,z}^*}{15\pi^2\hbar^3(-i\omega_s + \gamma)} \left[\frac{\frac{1}{i\omega_2+\gamma} + \frac{1}{-i\omega_1+\gamma}}{(-i(\omega_1 - \omega_2) + \gamma)} + \frac{1}{(-i2\omega_1 + \gamma)(-i\omega_1 + \gamma)} \right]. \quad (9)$$

Note the resonance at $\omega_1 = \omega_2$. The absolute value of the third-order susceptibility $\chi^{(3)} = \frac{i\sigma^{(3)}}{\omega_s}$, which follows from Eq. (9), is plotted in Fig. 1 as a function of detuning $\delta\omega = \omega_2 - \omega_1$ for several values of ω_1. The magnitudes of $\chi^{(3)}$ are many orders of magnitude higher as compared to typical values in the conventional nonlinear crystals [35]. Moreover, the numerical results in Fig. 1 and other figures below were obtained for $g_w = 4$, i.e., two pairs of Weyl points. Even higher nonlinearity and the nonlinear signal intensity are expected for larger values of g_w. However, strong optical absorption in WSMs limits the nonlinear signal power, as we show in the next section.

III. INTENSITY AND POWER OF THE FOUR-WAVE MIXING SIGNAL

As the simplest problem relevant to the experiment, we consider two monochromatic pump fields at frequencies ω_1 and ω_2 normally incident at the WSM layer from the air. The case of an oblique incidence can be easily solved in the same way, but we will try to keep the expressions less cumbersome. The nonlinear FWM signal at frequency $\omega_s = 2\omega_1 - \omega_2$ is generated by the nonlinear current inside the WSM material. It can be observed both in the transmission geometry, i.e., propagating through the WSM layer, or in the reflection geometry where it propagates away from the WSM surface into the air, opposite to the direction of the incident pump beam. Although there is no incident nonlinear signal, the presence of the "reflected" wave is mandated by the boundary conditions, since the nonlinear current exists only on one side of the air-WSM interface.

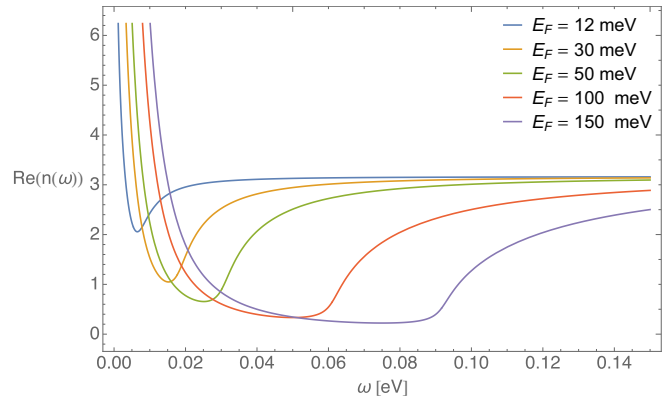

FIG. 2. Real (a) and imaginary (b) parts of the linear refractive index as a function of frequency at different Fermi energies for $\epsilon_b = 10$, $\hbar\gamma = 5$ meV, $v_F = 10^8$ cm/s, $g_s = 2$, $g_w = 4$.

First, it is instructive to find the linear dispersion and absorption of electromagnetic (EM) waves propagating in the bulk WSM. Since the material is isotropic within our model, the normal modes are transverse waves with the wave vector magnitude $k = \frac{n(\omega)\omega}{c}$. Here $n(\omega) = \sqrt{\epsilon(\omega)}$ and $\epsilon(\omega) = \epsilon_b + \frac{4\pi i\sigma^{(1)}}{\omega}$, where ϵ_b is the background dielectric permittivity due to off-resonant transitions to remote bands and $\sigma^{(1)}$ is the linear response of Weyl fermions given by Eq. (A7). The absorption length can be obtained as $L_{ab}(\omega) = \frac{c}{\omega \text{Im}[n]}$.

Figures 2 (a) and 2(b) show real and imaginary parts of the linear refractive index as a function of frequency at different Fermi energies. At low frequencies, the linear response is dominated by the plasmonic response of Weyl fermions. The plasmonic resonance $\text{Re}[\epsilon(\omega)] = 0$ is clearly visible in the refractive index spectra. Below the plasmonic resonance, the absorption length drops to the values shorter than the wavelength. Note that the plots cannot be applied to the interband transition region $\hbar\omega > 2E_F$.

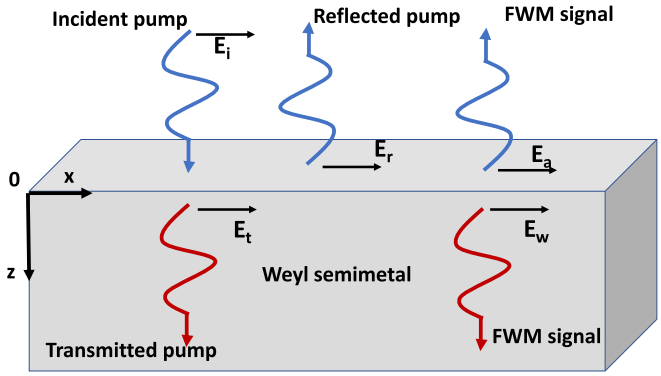

FIG. 3. Sketch of the simplest experimental geometry. The third-order nonlinear current generated in bulk WSM by incident pump beams gives rise to the FWM signals propagating both into and out of the material.

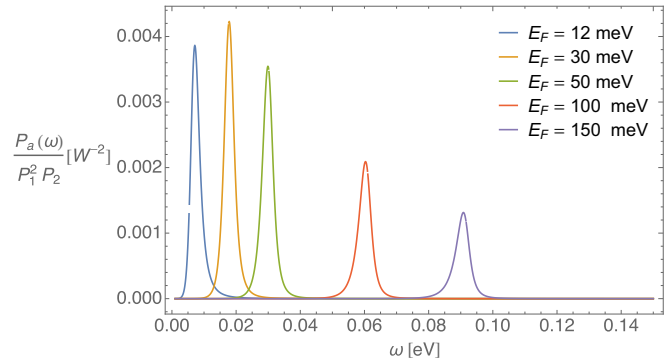

FIG. 4. The nonlinear signal power in reflection geometry, i.e., when the signal propagates away from the interface into the air, as a function of frequency and for several values of the Fermi energy.

Next, we calculate the intensity and power of the nonlinear signal. Assume that the interface between the WSM and the air is in the (x, y) plane and the WSM is at $z > 0$, as shown in Fig. 3. EM fields in the air above the WSM consist of incident and reflected pump waves, $E_{i1,2}e^{i(\omega_{1,2}/c)z}$ and $E_{r1,2}e^{-i(\omega_{1,2}/c)z}$, and the nonlinear signal wave propagating away from the interface: $E_a = E_a^{(-)}e^{-ik_0 z}$, where $k_0 = \omega_s/c$. Here we assume that all fields are linearly polarized in the same direction and drop the polarization vectors.

The EM fields in the WSM consist of transmitted pump waves $t_{1,2}E_{i1,2}e^{ik_{1,2}z}$, where $t_{1,2}$ are Fresnel transmission coefficients for the field at frequencies $\omega_{1,2}$, and the copropagating nonlinear signal. The nonlinear correction to the refractive index for the pump waves in the WSM is not important because they interact with the signal wave over a short distance comparable or smaller than the wavelength, as we will see below. The monochromatic electric field of the nonlinear signal at frequency ω_s satisfies Maxwell's wave equation with the nonlinear polarization $P^{(3)}(\omega_s)$ as the source term and appropriate boundary conditions for electric and magnetic fields at $z = 0$:

$$\frac{d^2E_w}{dz^2} + \epsilon(\omega_s)k_0^2 E_w = -\frac{4\pi\omega_s^2}{c^2}P^{(3)}(\omega_s). \tag{10}$$

After expressing the nonlinear polarization through the third-order susceptibility and the pump fields in the material, the right-hand side of Eq. (10) can be written as

$$\frac{d^2E_w}{dz^2} + \epsilon(\omega_s)k_0^2 E_w = Ae^{ikz}, \tag{11}$$

where $k \equiv 2k_1 - k_2$ and

$$A = -\frac{4\pi\omega_s^2}{c^2}\chi^{(3)}t_1^2 t_2^* E_{i1}^2 E_{i2}^*. \tag{12}$$

Note that the dielectric function $\epsilon(\omega)$ is complex at all frequencies and therefore all relevant wave numbers are complex: $k_{1,2} = (\omega_{1,2}/c)n_{1,2}$, $k_s = k_0 n_s$, where $n_{1,2} = \sqrt{\epsilon(\omega_{1,2})}$, $n_s = \sqrt{\epsilon(\omega_s)}$, and all imaginary parts $\mathrm{Im}[n_{1,2,s}]$ are greater than zero.

The solution to Eq. (11) can be written as a sum of the general solution to the homogeneous part and a particular solution to the inhomogeneous equation,

$$E_w = E_w^{(+)}e^{ik_s z} + \frac{A}{k_s^2 - k^2}e^{ikz}, \tag{13}$$

where we dropped the $E_w^{(-)}e^{-ik_s z}$ term.

The continuity of the tangential electric and magnetic fields at the interface $z = 0$ give $E_a = E_w$ and $\frac{dE_a}{dz} = \frac{dE_w}{dz}$, or

$$E_a^{(-)} = E_w^{(+)} + \frac{A}{k_s^2 - k^2},$$
$$-k_0 E_a^{(-)} = k_s E_w^{(+)} + k\frac{A}{k_s^2 - k^2}. \tag{14}$$

This leads to the following expressions for the nonlinear signal fields propagating from the interface into the air and into the WSM,

$$E_a = \frac{1}{k_s + k_0}\frac{A}{k_s + k}e^{-ik_0 z},$$
$$E_w = \frac{A}{k_s^2 - k^2}\left(e^{ikz} - \frac{k_0 + k}{k_0 + k_s}e^{ik_s z}\right), \tag{15}$$

where as a reminder $k = 2k_1 - k_2$. These expressions can be used to calculate the nonlinear signal power in both transmission and reflection geometry.

In the absence of any dissipation (i.e., when all wave numbers are real) and for exact phase matching $k_s \to k$, the monochromatic signal field propagating into the WSM grows linearly with z, as expected:

$$E_w = A\frac{e^{ik_s z}}{2k_s}\left(\frac{1}{k_0 + k_s} - iz\right), \quad E_a = \frac{A}{2k_s(k_s + k_0)}e^{-ik_0 z}. \tag{16}$$

Of course, for realistic fields of finite duration, the region of linear growth of the field is limited by the pulse duration. Moreover, field dissipation is always important because of a fast electron scattering rate γ expected in real materials and especially in the region around plasma resonance.

Figure 4 shows the power of the nonlinear signal in the reflection geometry, in W per W^3 of incident pump power, for degenerate FWM with $\omega_1 = \omega_2$ and assuming that all beams are focused into an area equal to vacuum wavelength squared,

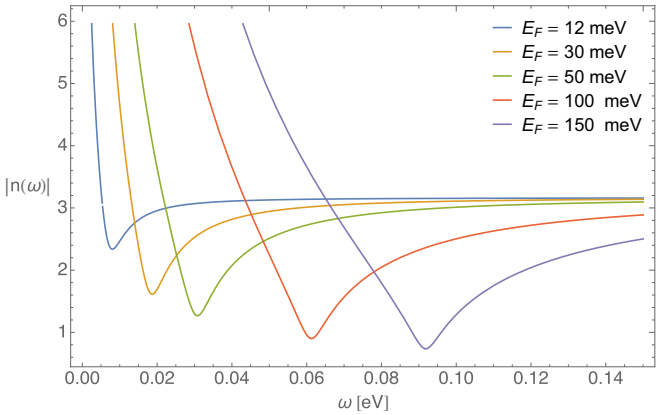

FIG. 5. Absolute value of the linear refractive index as a function of frequency at different Fermi energies for $\epsilon_b = 10$, $\hbar\gamma = 5$ meV, $v_F = 10^8$ cm/s, $g_s = 2$, $g_w = 4$.

i.e., $P_a = \frac{c}{2\pi}|E_a|^2(\frac{2\pi}{k_0})^2$ and similarly for the pump. All other parameters are the same as in Figs. 1 and 2.

The sharp peaks in the spectrum are entirely due to a strong dependence of the signal field intensity from the refractive index of the WSM:

$$|E_a|^2 = \frac{256\pi^2|\chi^{(3)}|^2}{|n_s|^2|n_s+1|^8}|E_i|^6. \quad (17)$$

Indeed, the absolute value of the refractive index has a sharp minimum in the vicinity of plasma resonance, see Fig. 5, which is manifested in the power spectra. Note a simple "universal" character of the expression Eq. (17) for the nonlinear signal, especially given the fact that the value of $\chi^{(3)}$ in this expression does not depend on the Fermi energy. The Fermi energy dependence in Eq. (17) which is shown in Fig. 4 enters entirely through the refractive index n_s.

The efficiency of the FWM process is quite high, a few mW per W^3 of incident pump power, especially in view of the fact that the reflected nonlinear signal is generated in the subwavelength skin layer below the air/WSM interface. It originates from the high magnitude of $|\chi^{(3)}|$ and strong refractive index dependence mandated by the boundary conditions. The sharp increase in the FWM signal near plasma resonance is conceptually similar to the predicted and observed enhancement of the third-order nonlinear effects for intense laser field propagating in epsilon-near-zero materials; see, e.g., Refs. [28,29] or the recent reviews [36,37] and references therein.

With detuning from resonance $\delta\omega = \omega_2 - \omega_1 = 0$, the FWM power will decrease following $|\chi^{(3)}|^2 \propto 1/(\delta\omega)^2$ as one can see from Eq. (9) and Fig. 1.

The field intensity of the transmitted nonlinear signal in the degenerate FWM process at the distance z into the sample is given by

$$|E_w|^2 = \frac{256\pi^2|\chi^{(3)}|^2|E_i|^6}{|n_s|^2|n_s+1|^6}\left|\frac{1}{1+n_s} - ik_0 z\right|^2 e^{-2k_0\mathrm{Im}[n_s]z}. \quad (18)$$

The corresponding power after propagating the distance equal to the absorption length $L_{ab} = 1/\mathrm{Im}[k_s]$ into the sample is plotted in Fig. 6 as a function of frequency for different

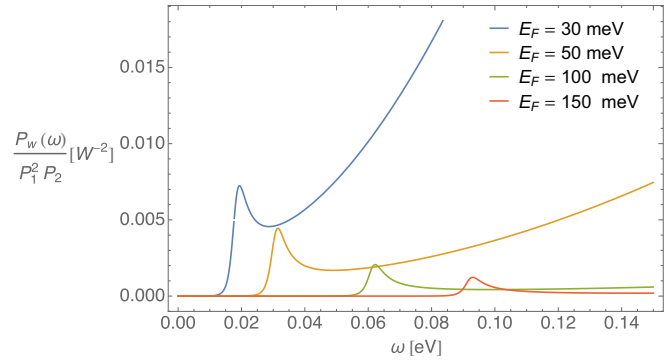

FIG. 6. The nonlinear signal power after propagating a distance equal to one absorption length $L_{ab} = 1/\mathrm{Im}[k_s]$ into the sample, as a function of frequency and for several values of the Fermi energy.

Fermi energies. Here we again assumed that the pump beam was focused into the area of $(2\pi/k_0)^2$.

The characteristic feature of each spectrum is a sharp peak just above plasma resonance, when the refractive index $n_s(\omega)$ is still close to its minimum value, followed by a gradual increase. The gradual increase is entirely due to the absorption length increasing with frequency, as shown in Fig. 7. Note, however, that the plots in Figs. 6 and 7 cannot be extended beyond $\omega = 2E_F$ where the interband transitions become important.

Therefore, for a sample with a given electron density, one can get similar levels of the transmitted nonlinear signal power when using a very thin film at frequencies near the plasma resonance and when using thicker films at higher frequencies near the interband transition cutoff. This is illustrated in Fig. 8 which shows the nonlinear signal power as a function of distance into the sample at two different frequencies and the same Fermi level.

Various strategies can be employed to extract the transmitted nonlinear signal from the sample on the bottom side of the WSM film: an index-matching substrate, tailoring the layer thicknesses to form a Fabry-Perot cavity or a coupled cavity, etc. We won't go into these technical details here. Moreover, since the magnitudes of the signal power in transmission and reflection geometries are similar (compare Figs. 4 and

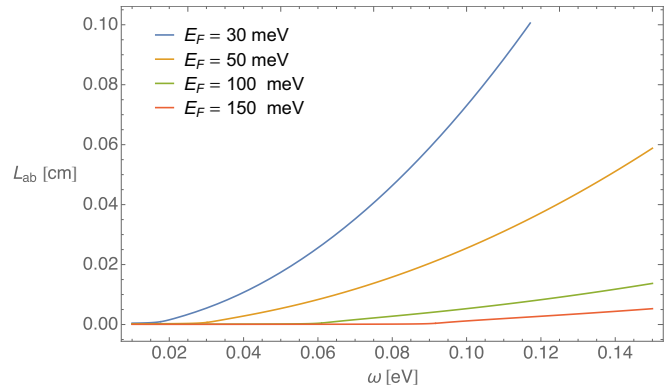

FIG. 7. Absorption length $L_{ab} = 1/\mathrm{Im}[k_s]$ as a function of frequency at different Fermi energies for $\epsilon_b = 10$, $\hbar\gamma = 5$ meV, $v_F = 10^8$ cm/s, $g_s = 2$, $g_w = 4$.

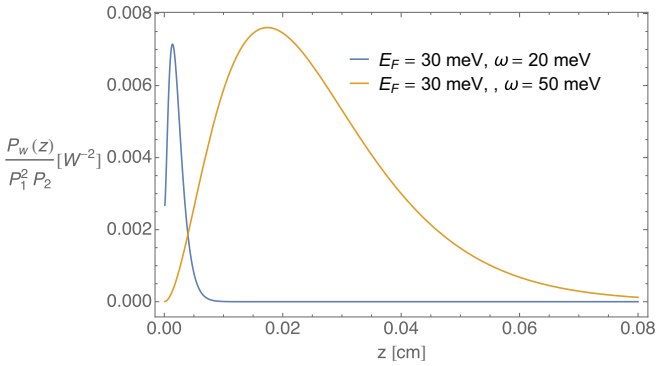

FIG. 8. The nonlinear signal power as a function of distance z into the sample at two different frequencies and the same Fermi energy.

8), in many cases it is more convenient to use the reflected (backward-propagating) FWM signal $|E_a|^2$ which is formed in the subwavelength layer of the order of skin depth at the surface. Then the details of the substrate and actual sample thickness don't matter, as long as this thickness is much larger than the skin depth. Since the electric field decays exponentially into the sample over the scale of the skin depth, the structure of the sample at several or more skin depths below the surface can't affect the signal.

IV. CONCLUSIONS

We studied the nonlinear optical response of WSMs within the kinetic equation approach which is valid at low enough frequencies in the vicinity of Weyl nodes and below the onset of interband transitions. We calculated the intensity of the nonlinear FWM signal in both transmission and reflection geometry. The doped bulk WSM exhibits extremely high third-order nonlinearity combined with very high absorption loss. This led us to rethink the optimal strategies for nonlinear signal generation. The nonlinear signal intensity is maximized in the vicinity of bulk plasma resonance, which allows one to use ultrathin WSM films of the order of skin depth. The nonlinear generation efficiency turns out to be quite high for a thin film of a highly dissipative material: of the order of several mW per W[3], in both transmission and reflection geometries. This could pave the way to interesting optoelectronic applications.

ACKNOWLEDGMENTS

This work has been supported in part by the Air Force Office for Scientific Research through Grant No. FA9550-17-1-0341 and by NSF Award No. 1936276. M.T. acknowledges the support from RFBR Grant No. 18-29-19091mk and the Federal Research Center Institute of Applied Physics of the Russian Academy of Sciences (Project No. 0035-2019-004).

APPENDIX: NONLINEAR OPTICAL CONDUCTIVITY DERIVATION

Substituting Eqs. (5) and (6) in the main text into Eq. (3) and transforming into spherical coordinates, one can write Eq. (3) in the following form:

$$\xi_n = \sum_{m,k} G^{n,m}\xi_k. \tag{A1}$$

The summation in Eq. (A1) is over all frequencies ω_m and ω_k that satisfy the condition $\omega_m + \omega_k = \omega_n$. The operator $G^{n,m}$ is determined by

$$G^{n,m}(p,\phi,\theta) \equiv g_1^{n,m}(\phi,\theta)\frac{\partial}{\partial p} + g_2^{n,m}(\phi,\theta)\frac{\partial}{p\partial\phi} + g_3^{n,m}(\phi,\theta)\frac{\partial}{p\partial\theta}, \tag{A2}$$

where p, ϕ, θ are spherical coordinates in momentum space and

$$g_1^{n,m} \equiv e\frac{E_{m,x}\cos\phi\sin\theta + E_{m,y}\sin\phi\sin\theta + E_{m,z}\cos\theta}{-i\omega_n + \gamma}, \tag{A3}$$

$$g_2^{n,m}(\phi,\theta) \equiv e\frac{E_{m,y}\cos\phi - E_{m,x}\sin\phi}{\sin\theta(-i\omega_n + \gamma)}, \tag{A4}$$

$$g_3^{n,m}(\phi,\theta) \equiv (E_{m,x}\cos\phi\cos\theta + E_{m,y}\sin\phi\cos\theta - E_{m,z}\sin\theta) \times\frac{e}{(-i\omega_n + \gamma)}. \tag{A5}$$

The optical response in any order for an arbitrary nondegenerate multiwave mixing can be calculated by the repetitive applying of $G^{n,m}$ to the equilibrium distribution function. For example, the first-order approximation describing the linear optical response is

$$\xi_n^{(1)} = G^{n,n}\xi_0 = g_1^{(n,n)}\frac{\partial F}{\partial p}. \tag{A6}$$

Substituting this into Eq. (4) and using $\int_0^\infty \frac{\partial F(p)}{\partial p}p^2 dp = -p_F^2$ in the strong degeneracy/low-temperature limit, one can get

$$\sigma^{(1)}(\omega) = \frac{e^2 v_F p_F^2 g_s g_w}{6\pi^2\hbar^3(\gamma - i\omega)}, \tag{A7}$$

where g_s and g_w are the degeneracy factors associated with spin and the number of Weyl nodes, respectively.

The second-order approximation of the nonequilibrium distribution function is $\xi_l^{(2)}$,

$$\xi_l^{(2)} = \sum_{m,k} G^{l,m}\xi_k^{(1)} = \sum_{m,k} G^{l,m}G^{k,k}\xi_0 \tag{A8}$$

for all possible ω_m and ω_k satisfying the relation $\omega_l = \omega_m + \omega_k$. Similarly, the third-order response is described by

$$\xi_i^{(3)} = \sum_{j,m,k} G^{i,j}\xi_l^{(2)} = \sum_{j,m,k} G^{i,j}G^{l,m}G^{k,k}\xi_0 \tag{A9}$$

for all possible ω_j, ω_m and ω_k satisfying the relation $\omega_i = \omega_j + \omega_m + \omega_k$.

To evaluate Eq. (A9)for the third-order perturbation of the distribution function, we need to calculate $G^{(n_3,m_3)}G^{(n_2,m_2)}g_1^{(n_1,m_1)}\frac{\partial F}{\partial p}$. First, by acting with $G^{(n_2,m_2)} \equiv G^2$ on $g_1^{(n_1,m_1)}\frac{\partial F}{\partial p} = g_1^1\frac{\partial F}{\partial p}$, we obtain

$$G^2 g_1^1\frac{\partial F}{\partial p} = g_1^2 g_1^1\partial_{p^2}^2 F + g_2^2\partial_\phi g_1^1\frac{\partial_p F}{p} + g_3^2\partial_\theta g_1^1\frac{\partial_p F}{p}. \tag{A10}$$

Second, acting with $G^{(n_3,m_3)} = G^3$ on Eq. (A10), we get

$$G^3G^2g_1^1\frac{\partial F}{\partial p} = \left(g_1^3\partial_p + g_2^3\frac{\partial_\phi}{p} + g_3^3\frac{\partial_\theta}{p}\right)\left(g_1^2g_1^1\partial_{p^2}^2F + \sin^2\theta g_2^2g_2^1\frac{\partial_pF}{p} + g_3^2g_3^1\frac{\partial_pF}{p}\right). \tag{A11}$$

The nonlinear current $\mathbf{j}^{(\omega_n=\omega_1+\omega_2+\omega_3)}$ is then given by

$$\begin{aligned}\begin{pmatrix} j_x^{\omega_n} \\ j_y^{\omega_n} \\ j_z^{\omega_n}\end{pmatrix} &= -ev_F\int_0^\infty\int_0^{2\pi}\int_0^\pi \xi_n^{(3)}\begin{pmatrix}\cos\phi\sin\theta\\ \sin\phi\sin\theta\\ \cos\theta\end{pmatrix}p^2\sin\theta d\theta d\varphi dp \\ &= \frac{1}{3!}\left(I_i^{3,2,1} + \text{Permutation}(\omega_1,\omega_2,\omega_3)\right),\end{aligned} \tag{A12}$$

where

$$\begin{aligned}I_i^{3,2,1} &= -ev_F\int_0^\infty\int_0^{2\pi}\int_0^\pi G^3G^2g_1^1\frac{\partial F}{\partial p}\begin{pmatrix}\cos\phi\sin\theta\\ \sin\phi\sin\theta\\ \cos\theta\end{pmatrix}p^2\sin\theta d\theta d\phi dp \\ &= \frac{8\pi e^4v_FF(0)}{15(\gamma-i\omega_1)(\gamma-i(\omega_1+\omega_2))}\frac{\Delta_{ijkl}E_1^jE_2^kE_3^l}{(\gamma-i(\omega_1+\omega_2+\omega_3))},\end{aligned} \tag{A13}$$

where $\Delta_{ijkl} = \delta_{ij}\delta_{kl} + \delta_{ik}\delta_{jl} + \delta_{il}\delta_{jk}$ and δ_{ij} is the Kronecker delta. Here we used the relations $\int_0^\infty \frac{\partial F(p)}{p^2\partial p}p^2dp = -\int_0^\infty \frac{\partial^2F(p)}{p\partial p^2}p^2dp = -F(0)$ and $\int_0^\infty \frac{\partial^3F(p)}{\partial p^3}p^2dp = -\int_0^\infty \frac{\partial(\frac{\partial F(p)}{p\partial p})}{\partial p}p^2dp = -2F(0)$. The summation over repeating indices is assumed.

For a strongly Fermi-degenerate distribution, we can replace the equilibrium distribution function with its zero-temperature limit, $F(p) = F(0)\Theta(p_F - p)$, where $F(0) = \frac{g_sg_w}{(2\pi\hbar)^3}$. Here g_s and g_w are the spin and Weyl node degeneracy, respectively. In this case, Eq. (A12) becomes

$$j_i(\omega_n) = \sigma_{ijkl}E_1^jE_2^kE_3^l, \tag{A14}$$

where

$$\sigma_{ijkl} = \frac{1}{3!}\left(\frac{8\pi e^4v_Fg_sg_w\Delta_{ijkl}}{15(2\pi\hbar)^3(\gamma-i\omega_1)}\frac{1}{[\gamma-i(\omega_1+\omega_2)][\gamma-i(\omega_1+\omega_2+\omega_3)]} + \text{Permutation}(\omega_1,\omega_2,\omega_3)\right) \tag{A15}$$

is the third-order nonlinear optical conductivity at zero temperature.

[1] X. Wan, A. M. Turner, A. Vishwanath, and S. Y. Savrasov, Phys. Rev. B **83**, 205101 (2011).

[2] A. A. Burkov and L. Balents, Phys. Rev. Lett. **107**, 127205 (2011).

[3] S.-Y. Xu, I. Belopolski, N. Alidoust, M. Neupane, G. Bian, C. Zhang, R. Sankar, G. Chang, Z. Yuan, C.-C. Lee, S.-M. Huang, H. Zheng, J. Ma, D. S. Sanchez, B. Wang, A. Bansil, F. Chou, P. P. Shibayev, H. Lin, S. Jia, and M. Z. Hasan, Science **349**, 613 (2015).

[4] B. Q. Lv, H. M. Weng, B. B. Fu, X. P. Wang, H. Miao *et al.*, Phys. Rev. X **5**, 031013 (2015).

[5] B. Yan and C. Felser, Annu. Rev. Condens. Matter Phys. **8**, 337 (2017).

[6] M. Z. Hasan, S.-Y. Xu, I. Belopolski, and S.-M. Huang, Annu. Rev. Condens. Matter Phys. **8**, 289 (2017).

[7] N. P. Armitage, E. J. Mele, and A. Vishwanath, Rev. Mod. Phys. **90**, 015001 (2018).

[8] A. A. Burkov, Annu. Rev. Condens. Matter Phys. **9**, 359 (2018).

[9] M. Kargarian, M. Randeria, and N. Trivedi, Sci. Rep. **5**, 12683 (2015).

[10] C. J. Tabert and J. P. Carbotte, Phys. Rev. B **93**, 085442 (2016).

[11] J. Hofmann and S. Das Sarma, Phys. Rev. B **91**, 241108(R) (2015).

[12] M. S. Ukhtary, A. R. T. Nugraha, and R. Saito, J. Phys. Soc. Jpn. **86**, 104703 (2017).

[13] S.-i. Kimura, H. Yokoyama, H. Watanabe, J. Sichelschmidt, V. Suß, M. Schmidt, and C. Felser, Phys. Rev. B **96**, 075119 (2017).

[14] O. V. Kotov and Yu. E. Lozovik, Phys. Rev. B **98**, 195446 (2018).

[15] G. M. Andolina, F. M. D. Pellegrino, F. H. L. Koppens, and M. Polini, Phys. Rev. B **97**, 125431 (2018).

[16] K. Halterman, M. Alidoust, and A. Zyuzin, Phys. Rev. B **98**, 085109 (2018).

[17] H. Rostami and M. Polini, Phys. Rev. B **97**, 195151 (2018).

[18] Q. Chen, A. R. Kutayiah, I. Oladyshkin, M. Tokman, and A. Belyanin, Phys. Rev. B **99**, 075137 (2019).

[19] C. A. C. Garcia, J. Coulter, and P. Narang, Phys. Rev. Research **2**, 013073 (2020).

[20] J. Ma, Q. Gu, Y. Liu, J. Lai, P. Yu, X. Zhuo, Z. Liu, J.-H. Chen, J. Feng, and D. Sun, Nat. Mater. **18**, 476 (2019).

[21] J. Moore, Nat. Sci. Rev. **6**, 206 (2019).

[22] Q. Chen, M. Erukhimova, M. Tokman, and A. Belyanin, Phys. Rev. B **100**, 235451 (2019).
[23] I. D. Tokman, Q. Chen, I. A. Shereshevsky, V. I. Pozdnyakova, I. Oladyshkin, M. Tokman, and A. Belyanin, Phys. Rev. B **101**, 174429 (2020).
[24] R. Okugawa and S. Murakami, Phys. Rev. B **89**, 235315 (2014).
[25] C. K. N. Patel, R. E. Slusher, and P. A. Fleury, Phys. Rev. Lett. **17**, 1011 (1966).
[26] P. A. Wolff and G. A. Pearson, Phys. Rev. Lett. **17**, 1015 (1966).
[27] C. C. Wang and N. W. Ressler, Phys. Rev. **188**, 1291 (1969).
[28] A. Capretti, Y. Wang, N. Engheta, and L. D. Negro, Opt. Lett. **40**, 1500 (2015).
[29] M. Z. Alam, I. D. Leon, and R. W. Boyd, Science **352**, 795 (2016).
[30] Z. Sun, D. N. Basov, and M. M. Fogler, Phys. Rev. B **97**, 075432 (2018)
[31] Y. Zhong, W. Feng, Z. Liu, C. Zhang and, J. C. Cao, Physica B: Condensed Matter **555**, 81 (2019).
[32] J. W. Zuber, T. Zhao, S. Gong, M. Hu, R. B. Zhong, C. Zhang, and S. G. Liu, Phys. Rev. B **101**, 085307 (2020).
[33] Y. Wang, M. Tokman, and A. Belyanin, Phys. Rev. B **94**, 195442 (2016).
[34] T. Jiang, V. Kravtsov, M. Tokman, A. Belyanin, and M. Raschke, Nature Nano **14**, 838 (2019).
[35] R. W. Boyd, *Nonlinear Optics* (Academic Press, London, 2003).
[36] O. Reshef, I. D. Leon, M. Z. Alam, and R. W. Boyd, Nat. Rev. Mater. **4**, 535 (2019).
[37] N. Kinsley and J. Khurgin, Opt. Mat. Express **9**, 2793 (2019).